DESIGN, MODELING AND REALIZATION OF SPIRAL INDUCTOR

Submitted in partial fulfilment of the Degree of

Bachelor of Technology

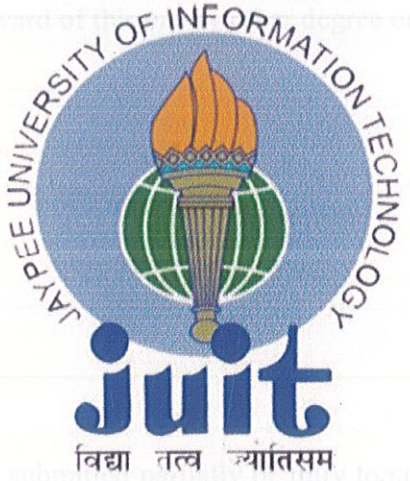

2011-12

ENROLMENT. NO.	NAME
081001	SIDDHARTH GARG
081009	SANSKAR DEEPAK
081013	SAMAR MANKOTIA

Name of supervisor- **Prof. Dr. Sunil V Bhooshan**

DEPARTMENT OF ELECTRONICS AND COMMUNICATION ENGINEERING

JAYPEE UNIVERSITY OF INFORMATION TECHNOLOGY,

WAKNAGHAT

CERTIFICATE

This is to certify that project report entitled **DESIGN, MODELING AND REALIZATION OF SPIRAL INDUCTOR**, submitted by **SIDDHARTH GARG, SANSKAR DEEPAK** and **SAMAR MANKOTIA** in partial fulfilment for the award of degree of Bachelor of Technology in Electronics and Communication Engineering to Jaypee University of Information Technology, Waknaghat, Solan has been carried out under my supervision. This work has not been submitted partially or fully to any other University or Institute for the award of this or any other degree or diploma.

Date: 31/5/2012

Prof. Dr. Sunil V Bhooshan

H.O.D. (ECE)

Certified that this work has not been submitted partially or fully to any other University or Institute for the award of this or any other degree or diploma.

Siddharth Garg

(081001)

Sanskar Deepak

(081009)

Samar Mankotia

(081013)

ACKNOWLEDGEMENT

It has been wonderful and intellectually stimulating experience working on **DESIGN, MODELING AND REALIZATION OF SPIRAL INDUCTOR.**

We gratefully acknowledge the Management and Administration of Jaypee University of Information Technology for providing us the opportunity and hence the environment to initiate and complete our project.

For providing with finest details of the subject, we are greatly thankful to our project guide **Prof. Dr. Sunil Bhooshan**. He has provided us the way to get the job done, not providing the exact way to do it, but the concept behind the complexities so that we can make better use of the existing knowledge and build up higher skills to meet the industry needs. His methodology of making the system strong from inside has taught us that output is not end of project.

Date: 31/5/2012

SIDDHARTH GARG(081001)

SANSKAR DEEPAK (081009)

SAMAR MANKOTIA (081013)

TABLE OF CONTENTS

SUMMARY

Integrated inductors also called as spiral inductors, on-chip inductors or planar inductors are inseparable part in radio frequency integrated circuits (RFICs). Increasing growth in RFICs from the past few decades has forced study of these components in greater detail. Apart from IC conductors there are several components mounted on a chip - namely capacitors, resistors, MOSFETs, diodes etc. It is extremely important to understand the electrical and magnetic behaviour of all these components. Electrical behaviour of these components is easy to understand. However, the real challenge lays in realizing and predicting the magnetic behaviour of components namely, inductors and capacitors. Capacitors have their own physical model developed for accurate modelling, but for inductors there are many factors to be considered. As the frequencies in RFICs are in the GHz range, factors such as self-resonant frequency (*SRF*), quality factor (*Q*), self and mutual inductance are critical to design due to the very small size of inductor. This project concentrates on a brief study of integrated inductors, their construction and modelling and presents a novel way to estimate inductance on spiral inductor using **"Equivalent Radius Method".** Present project in this field will make it possible to predict magnetic behaviour accurately by theoretical methods.

Sanskar Deepak
Samar Mankotia

Signature of Student

Name SIDDHARTH GARG, SANSKAR DEEPAK, SAMAR MANKOTIA

Date 31/5/2012

Signature of Supervisor

Name Prof. Dr. S. V Bhooshan

Date 31/5/12

LIST OF FIGURES

LIST OF SYMBOLS AND ACRONYMS

$\mathbf{E}$	Electric field
$\mathbf{B}$	Magnetic flux density (also called magnetic field)
$\mathbf{H}$	Magnetizing field
$\mathbf{J_c}$	Conduction current density
$\mathbf{J_d}$	Displacement current density
$\mathbf{J}$	Total current density
$\mathbf{D}$	Electric displacement field
ρ	Volume charge density
ρ_s	Surface charge density
ε	Electric permittivity
μ	Magnetic permeability
σ	Electric conductivity
∇	Differential operator Nabla
∇f	Gradient of f
$\nabla \cdot \mathbf{a}$	Divergence of $\mathbf{a}$
$\nabla \times \mathbf{a}$	Rotational of $\mathbf{a}$

CHAPTER 1

INTRODUCTION

With the emergence of cellular phone, wireless local-area network (WLAN) and Bluetooth technology, we are standing on the threshold of a new radio frequency epoch. Compared with the old epoch dominated by discrete bipolar transistors and discrete filters, the new epoch is remarkable for the development of radio frequency integrated circuits (RF ICs), especially Si RF ICs, which are cheaper to fabricate and easier to integrate than GaAs ICs. In the new epoch, most of the radio transceiver components, such as low noise amplifiers (LNA), mixers, oscillators and filters will be integrated on one monolithic chip, sometimes with digital baseband circuits as system-on-a-chip (SOC). By doing this, the cost and the difficulty of assembly and tuning are reduced drastically.

The integrated spiral inductor plays an important role in the development of Si RF ICs. As pointed out in [1], the first published integrated CMOS RF amplifier was hidden in a paper on fabricating a suspended spiral inductor on silicon [2] in 1993. This is because a source-degenerating inductor has to be used to tune the transistor capacitance to obtain gain at RF frequency. This inductor has to be built on-chip so that the parasitic capacitance coming with the off-chip inductor does not ruin the performance of the amplifier. The spiral inductor has a great influence on the performance of many RF circuits. The obvious example is the LC tank, in which the quality factor Q of the spiral inductor determines the bandwidth and the resonance impedance of the LC tank. Another example is the bandpass filter (BPF) built with inductors and capacitors, in which the quality factor of the spiral inductor determines the insertion loss [3]. In low noise

amplifiers (LNA), the quality factor of the spiral inductor determines the figure of merit (FoM), which is the measure of the overall performance of the LNA [3]. In voltage controlled oscillators (VCO), high-Q spiral inductors reduce both DC power consumption and phase noise [3].

The spiral inductor was once thought to be impractical to be built on heavily doped silicon due to large substrate losses. This situation changed since 1990s, when the first spiral inductor built on silicon was reported [4]. In 1993, a 100-nH suspended on-chip spiral inductor was fabricated by removing the silicon substrate under the spiral inductor [2]. In 1995, a multi-layer spiral inductor was proposed and fabricated [5][6]. In 1996, high-resistivity silicon was used to reduce the substrate loss [7]. In 1998, a patterned ground shield between the spiral inductor and silicon substrate was introduced to separate the electric field of the spiral inductor from the substrate [8]. By the late 1990s, the effort to suspend the spiral inductor from the substrate using MEMS (Microelectromechanical Systems) technology [9]-[11] gradually developed into a new field by its own: RF MEMS [12].

At the same time, a lot of work has been done in the synthesis and optimization of spiral inductors on silicon. Most of these works are based on circuit models. In [21], an analytical design procedure based on the physical model is presented. In [22] and [23], geometric programming (GP) formulation of the spiral inductor optimization is proposed, based on the model presented in [16]. In [24] and [25], sequential quadratic programming (SQP) and an optimization method called mesh adaptive direct search (MADS) are used to optimize the spiral inductor, both are based on circuit models. Although these methods are very efficient, the results they give depend on the quality of the circuit model they use. It is likely that the design does not meet the specification when validated by EM simulators or measurements. Thus direct

optimization based on more accurate EM simulators is highly desirable. Unfortunately, the task is extremely time-consuming, if not impossible, with current computational power. To address this problem, Bandler *et al.* introduced space mapping (SM) technology [20]-[23] in 1994 to incorporate the computational efficiency of cheap circuit models and the accuracy of expensive EM simulations. Space mapping algorithms perform optimization on a cheap circuit model and use EM simulations to calibrate the circuit model. Reviews of recent developments of space mapping technology are given in [28] and [29]. **The purpose of this project is to present an optimization method for the design of spiral inductors and LC resonators using the "Equivalent Radius Method".**

The objective of this work is to develop a theoretical method which can predict the self and mutual inductance values of certain inductor geometries with reasonable accuracy and speed in order to be able to decide the optimal inductor geometry to implement in wireless devices. Several methods were explored to decide which approach would solve the problem reliably and elegantly. The primary factors considered were efficiency, simplicity and computational speed. The equivalent radius method satisfied all three criteria and seemed to be the best way to proceed for a variety of reasons. As it turns out, the equivalent radius method, like most other inductance calculation methods, can theoretically find out the inductance values of any given structure. However, for the specific structures we are interested in, the equivalent radius method simplifies the problem greatly due to the symmetry and regularity of the geometries under investigation. This greatly reduces the complexity of the problem.

CHAPTER 2

RECENT WORK ON THE MODELING AND OPTIMIZATION OF SPIRAL INDUCTORS ON SILICON

2.1 INTRODUCTION

Inductors are components used to store energy in the form of magnetic fields. In RF integrated circuits, inductors of spiral shape are fabricated on metal layers. As an example, the top and sectional view of a square inductor fabricated in a sample CMOS process are shown in Fig. 2.1 and Fig. 2.2. Two metal layers are used: the top layer for the spiral inductor and the lower layer for the underpass (the part shown by the dotted line in Fig. 2.1). The geometry parameters of the spiral inductor are the number of turns n, the width of the metal trace w, the turn spacing s, the inner diameter din and the outer diameter d_{out}.

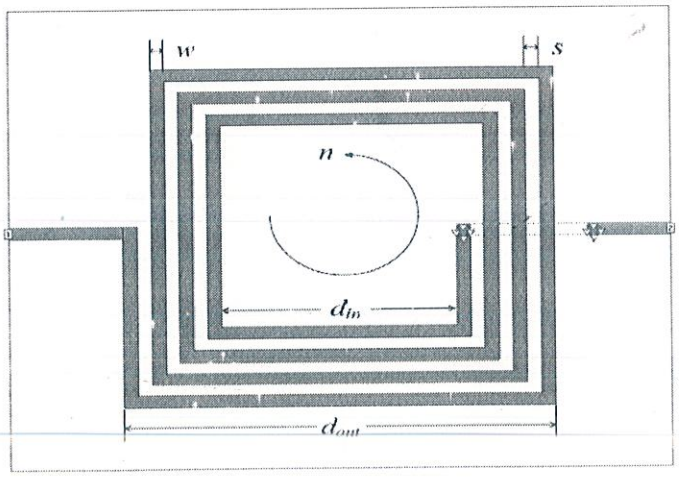

Fig. 2.1 Square spiral inductor (top view) [1].

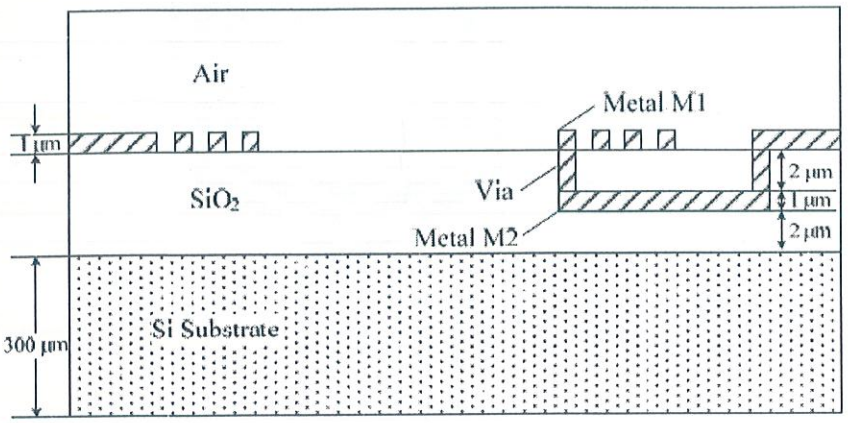

Fig. 2.2 Square spiral inductor (sectional view) [1].

Spiral inductors can be fabricated in other shapes. Fig. 2.3 shows spiral inductors in hexagonal, octagonal and circular shapes. In order to enhance the quality factor, multi-level metal layers are sometimes connected in parallel to fabricate the spiral inductor [3]. For the same purpose, the patterned ground shield (PGS) made with the metal layer between the spiral inductor and the substrate can be used (Fig. 2.4).

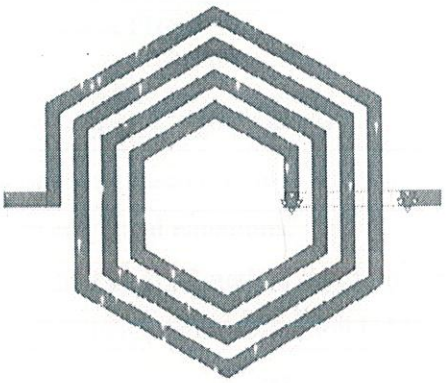

(a)

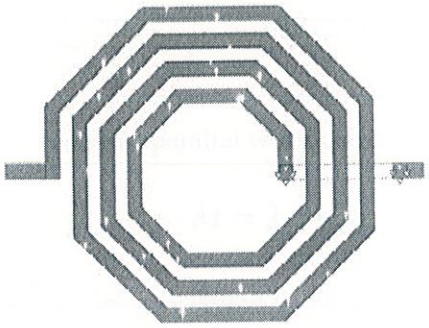

(b)

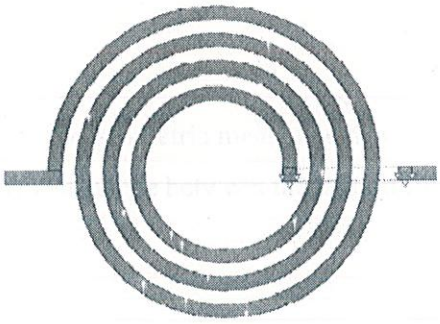

(c)

Fig. 2.3 Spiral inductor: (a) hexagonal, (b) octagonal, and (c) circular.

2.2 INDUCTANCE CALCULATION

Many methods have been proposed to calculate the inductance L_s and they can be divided into two categories. The first ones are based on the self and mutual inductance calculation for single wires. The second ones are empirical equations.

The basic equations for the first kind of method are summarized in [8]. In particular, the self-inductance of a wire with a rectangular cross-section is [7] where L_{self} is the self-inductance in

$$L_{self} = 2l \cdot (\ln \frac{2l}{w+t} + 0.5 + \frac{w+t}{3l}) \qquad (2.2.1)$$

nH, l is the wire length in cm, w is the wire width in cm and t is the wire thickness in cm. This equation only applies when the wire length is greater than approximately twice the cross-section dimension.

The mutual inductance between two parallel wires can be expressed as [7] where M is the

$$M = 2 \cdot l \cdot Q_m \qquad (2.2.2)$$

mutual inductance in nH, l is the wire length in cm and Q_m is the mutual inductance parameter

$$Q_m = \ln\left[\frac{l}{GMD} + \sqrt{1+(\frac{l}{GMD})^2}\right] - \sqrt{1+(\frac{GMD}{l})^2} + \frac{GMD}{l}. \qquad (2.2.3)$$

The GMD in (2.9) refers to the geometric mean distance between wires. It is approximately equal to the pitch of the wires (the distance between the central line of the wire). A more precise definition for GMD is [7]

$$\ln GMD = \ln d - \frac{w^2}{12d^2} - \frac{w^4}{60d^4} - \frac{w^6}{168d^6} - \frac{w^8}{360d^8} - \frac{w^{10}}{660d^{10}} - \cdots \qquad (2.2.4)$$

Where d is the pitch of the wires and w is the width of the wires.

Based on (2.2.1) and (2.2.4), Greenhouse proposed a method to calculate the inductance of the spiral inductor [9]. As shown in Fig. 2.7, the spiral inductor is divided into single wires. The inductance of the spiral inductor is then calculated from the self-inductances and the mutual inductances of these wires. The general equation for this calculation is [9]

$$L_T = L_0 + M_+ - M_- \qquad (2.2.5)$$

Where L_T is the total inductance of the spiral inductor, L_0 is the sum of self-inductances, $M+$ is the sum of positive mutual inductances (when the current in two parallel wires is in the same direction) and $M-$ is the sum of negative mutual inductances (when the current in two parallel wires is in the opposite direction).As an example, the inductance for the spiral inductor in Fig. 2.7 can be calculated as

$$\begin{aligned} L_T = {} & L_1 + L_2 + L_3 + L_4 + L_5 + L_6 + L_7 + L_8 + 2(M_{1,5} + M_{2,6} + M_{3,7} \\ & + M_{4,8}) - 2(M_{1,7} + M_{1,3} + M_{5,7} + M_{5,3} + M_{2,8} + M_{2,4} + M_{6,8} \\ & + M_{6,4}) \end{aligned} \qquad (2.2.6)$$

where L_i is the self-inductance of the wire i and $M_{i,j}$ is the mutual inductance between wire i and wire j.

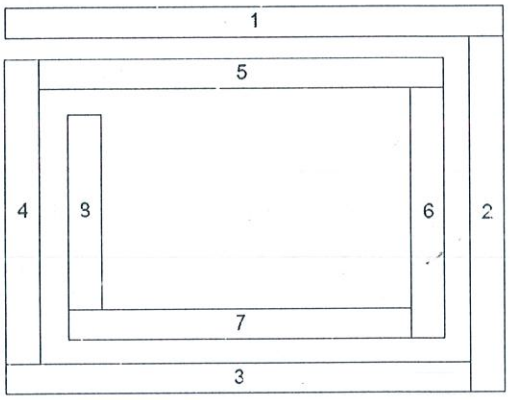

FIG 2.4 (Spiral inductor (as line segments))

CHAPTER 3

Electromagnetic Formulation and Inductor Specifications

Introduction

In this chapter we will discuss relevant electromagnetic theorems and assumptions. We begin with Ampere's Law, Faradays Law and discuss inductor specifications.

3.1 Inductive Interaction between Conductors

The process of inductive interaction between conductors carrying currents can be decomposed into three effects which take place concurrently [22]:

- Currents flowing through conductors create magnetic fields (Ampere's Law)
- Magnetic fields varying with time create induced electric fields (Faraday's Law)
- Induced electric fields exert forces upon the electrons in the conductors and cause electric voltage (Electric Potential) drops.

3.1.1 Ampere's Law

Currents flowing through conductor loops and time- varying electric fields create magnetic fields. This relationship between current density j, the electric field E and the resulting magnetic field B is Ampere's Law:

$$\nabla \times \mathbf{B} = \mu \mathbf{j} + \mu\epsilon \frac{\partial \mathbf{E}}{\partial t} \tag{3.1.1}$$

The first term on the right hand side of (3.1.1) represents the contribution of the current density to the magnetic field on the left hand side. μ is the magnetic permeability of the insulator surrounding the wires and its electric permittivity. The curl operator on the left hand side causes

the resulting magnetic field to be wrapped around the existing current flow patterns (see Fig. 3.1). The integral form, which can be derived from (1) via Stokes' Law, is

$$\oint_S \mathbf{B} \cdot \mathbf{dl} = \mu \int_S \left(\mathbf{j} + \epsilon \frac{\partial \mathbf{E}}{\partial t} \right) \cdot \mathbf{dS} \tag{3.1.2}$$

where S is a surface which intersects the wire (see Fig. 3.1). The current through the wire creates a magnetic field around the wire. For a general, three-dimensional current flow this field is

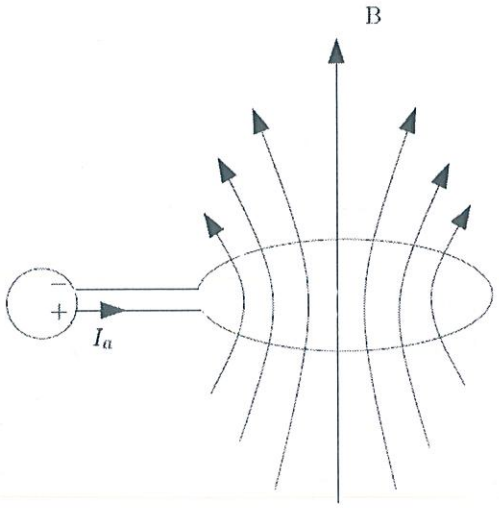

Figure 3.1: Magnetic Field created by time-variant current flowing through conductor loop

to predict intuitively, but for one-dimensional wires the field direction can be predicted with the right- hand rule: if the thumb of the right hand points in current direction, the other fingers point in direction of the magnetic field.

The second term in the right-hand side integral of (3.1.2) is referred to as the displacement current density, since it has the dimension of a current density and represents the ac current flowing between two conductors due to their capacitive couplings. Time-varying electric fields can create magnetic fields. Usually, however, this term is neglected in Ampere's Law for integrated circuits since the magnetic field created directly by the currents flowing within the

conductors is larger than the magnetic field created by the displacement currents - even with dominant lateral capacitance coupling - by at least one order of magnitude.

Discarding the displacement current term in (3.1.2) decouples the inductive and capacitive effects within the circuit; therefore this step is referred to as a quasi-static approximation, since the capacitive electric fields are assumed to be roughly (quasi) static and variations of the potential differences between conductors are sufficiently slow such that the displacement term is negligible compared with the current term. The quasi-static (differential and integral) form of Ampere's Law is:

$$\nabla \times \mathbf{B} = \mu \mathbf{j} \tag{3.1.3}$$

$$\oint_S \mathbf{B} \cdot \mathbf{dl} = \mu \int_S \mathbf{j} \cdot \mathbf{dS} \tag{3.1.4}$$

Though the displacement current contribution to the magnetic field is usually negligible, the displacement current itself, however, is not negligible. It may be shown that the contribution of the displacement currents to the magnetic field is negligible.

3.1.2 Faraday's Law

Ampere's Law gives us the first part of the inductive process: the creation of the magnetic field. Only if these magnetic fields vary with time do these fields create induced electric fields. Therefore, time-variant currents are required for induction, the relationship of which is Faraday's Law:

$$\oint_j \mathbf{E}_{\text{ind}} \cdot \mathbf{dl} = -\frac{\partial \phi}{\partial t} \tag{3.1.5}$$

Where $\phi = \int B.ds$ is the magnetic flux with the integral taken over the area of the primary loop and E_{ind} is the induced electric field in the secondary loop. The induced electric field wraps around the magnetic field lines (see Fig. 3.2). The portion of the induced electric field which is parallel

to the wire of the loop in Fig. 3.2 exerts force on the charges and creates voltage in the loop. The induced E-field is caused by the time-variant magnetic field in Eq. (3.1.4). The orientation of the loop with respect to the induced electric field determines the amount of induced voltage. If the loop is orthogonal to the induced E-field the total effect of the magnetic field on it will be zero (As we will see later in a more detailed derivation, this causes partial inductive couplings between orthogonal wires to become zero).

3.1.3 Electric Potential

The induced electric field can be integrated along the victim loop and results in an induced voltage which adds to the already existing voltage due to the resistance of the loop:

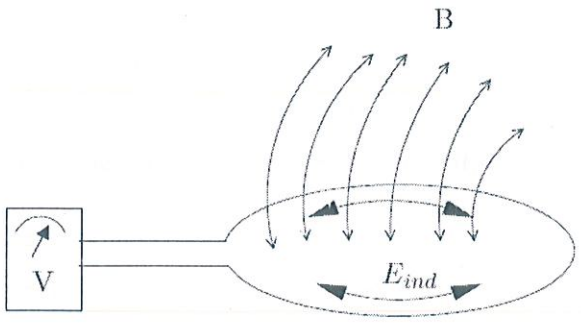

Figure 3.2: Electric Voltage created by time-variant magnetic field passing through a conductor loop

$$V_i^{ind} = -\oint_i \mathbf{E_{ind}} \cdot \mathbf{dl} \tag{3.1.6}$$

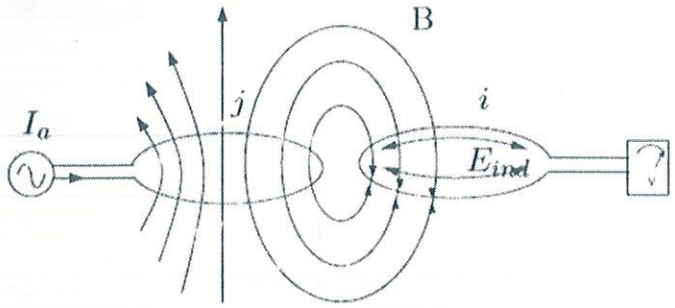

Figure 3.3: Magnetic Field created by the time-variant current in loop *j* induces voltage in loop *i*, since some of the magnetic field passes through *i*

3.1.4 Loop Inductance

Fig. 3.3 summarizes the combination of these three effects which combine to generate a voltage drop in the victim loop *i* due to a time-variant current in loop *j*. All three relationships involved in the preceding equations are linear. Therefore, the resulting combined relationship between time-derivatives of currents in the loops and the resulting induced voltage drop is linear as well:

$$V_i^{ind} = L_{ij}\frac{\partial I_j}{\partial t} \tag{3.1.7}$$

Where $I_j = \int j.dS$ and the integral is taken over the cross sectional area of conductor *j*.

L_{ij} is the mutual inductance of loop *j* upon loop *i* and I_j is the current flowing through the Loop *j*. V^{ind}_i is the voltage induced in the victim loop *i*. For the special case where loops *i* And *j* are the same, the coefficient L_{ii} is the self-inductance of loop *i*.

3.2Inductor Specifications

A current flowing through the conductor produces magnetic flux. This magnetic flux generates the electromotive force (EMF) proportional to the flow of current. Any change in current changes the magnetic flux. This in turn changes the EMF. Inductance is a measure of this change in EMF per unit change of current. Consider a single turn inductor carrying a 1 ampere current producing 1 volt EMF. Corresponding inductance (L) measured is 1 Henry (H). Now, if the number of turns is increased, the EMF varies and so does the inductance L. Some of the important specifications of an inductor are:

(a) Self Inductance

(b) Mutual Inductance

(c) Quality Factor

(a) Self-Inductance: Suppose there are two coils connected in series having a certain number of turns. Change of current in coil 1 causes change in magnetic flux linking with coil 2. Similarly, it causes change in its own magnetic flux linking with self turns. This changes the self-flux linkages, and is called as self-inductance of coil denoted by L. The flux linkage is given by

$$v(t) = -L\frac{di}{dt}. \tag{3.2.1}$$

(b) Mutual Inductance: Consider the same example as in case of self-inductance. The change in current flowing through coil 1 produces change in magnetic flux linking with the second coil. This causes a change in flux linkages of coil 2 and is called as mutual inductance denoted by M. The flux linkage is given by

$$v(t) = -M_{12}\frac{di}{dt}. \tag{3.2.2}$$

If there are multiple coils connected in series, the total inductance of a coil is given by

$$L_T = L_1 + L_2 + L_3 + \ldots\ldots + L_n \pm 2M_{12} + \ldots\ldots \tag{3.2.3}$$

The sign for mutual inductance in the above equation depends on whether EMF's are adding or subtracting with self EMFs. According to Lenz's law self EMFs always oppose the mutual EMFs indicating negative sign.

(c) *Quality Factor (Q):* An ideal inductor is lossless. The coil of an inductor is made of metal wire, which consists of some parasitic resistance. When current flows through the coil it causes heat loss due to series resistance, which deteriorates the quality of the inductor for a given design. Measure of heat loss is called as the quality factor of the inductor. It is given as ratio of inductive reactance to series resistance.

$$Q == \frac{\omega L}{R}. \tag{3.2.4}$$

CHAPTER 4

Calculation of Inductance Using Equivalent Radius Method

Consider a loop of radius R as shown in Figure 4.1 of circular cross- section, where *a* is the radius of the wire.

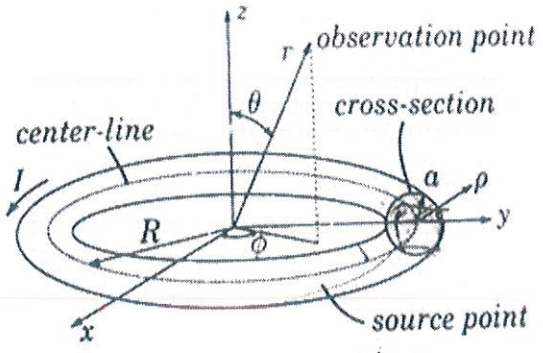

Figure 4.1: A circular loop of wire carrying a current I

The vector potential A near the wire is given by

$$A_i(\mathbf{r}) = \frac{\mu_0}{4\pi} \iiint_{V'} \frac{J_i(\mathbf{r}')dV'}{|\mathbf{r}-\mathbf{r}'|} \qquad i=x,y,z \tag{4.1}$$

Observing a point in the wire we can see that there is only component of J, namely J_ϕ and

$$\mathbf{J} = J_\phi\left(-\mathbf{a}_x \sin\phi' + \mathbf{a}_y \cos\phi'\right) \tag{4.2}$$

where J is the magnitude of the current density and is uniform throughout the cross- section

Writing Considering a point on the x-z plane where ϕ=0

$$|\mathbf{r} - \mathbf{r}'| = \sqrt{(x-x')^2 + (y-y')^2 + (z-z')^2}$$

$$= \sqrt{R^2 + r^2 - 2Rr\sin\theta\cos\varphi'} \tag{4.3}$$

$$A_x = \left(\frac{\mu_0}{4\pi}\right) IR \int_0^{2\pi} \frac{(-\sin\phi')d\phi'}{\sqrt{R^2 + r^2 - 2Rr\sin\theta\cos\phi'}} = 0$$

$$A_y = \left(\frac{\mu_0}{4\pi}\right) IR \int \frac{(\cos\phi')d\phi'}{\sqrt{R^2 + r^2 - 2Rr\sin\theta\cos\phi'}}$$

$$A_z = 0 \tag{4.4}$$

The first equation is zero since the integrand has odd symmetry about π, the second equation is not zero and is A_ϕ and the third equation is zero since J_z=0. The second equation can be expressed in terms of the complete elliptic integrals K and E,

Where $$A_\phi = \left(\frac{\mu_0}{4\pi}\right)\left(\frac{4IR}{\sqrt{R^2 + r^2 + 2Rr\sin\theta}}\right)\left[\frac{(2-k^2)K(k) - 2E(k)}{k^2}\right] \tag{4.5}$$

$$k^2 = \frac{4Rr\sin\theta}{R^2 + r^2 + 2Rr\sin\theta} \tag{4.6}$$

for r=R , $\theta=\pi/2$ we find that k≈1. On closer examination we discovered that K(k) becomes infinity but E(k) remains finite and ≈1. The functions near this point can be approximated by

$$K(z)|_{z\to 1} \approx -\frac{1}{2}\ln(1-z)\left(1-\frac{z-1}{4}+O((z-1)^2)\right)+\ln 4+\frac{1}{4}(1-\ln 4)(z-1)+O((z-1)^2) \tag{4.6}$$

$$E(z)|_{z\to 1} \approx 1+\frac{1}{2}\ln(1-z)\left(\frac{z-1}{4}\right)+\frac{z-1}{4}\left(-2\ln 4+1+O((z-1)^2)\right) \tag{4.7}$$

We can see from these equations that as z⟶ 1 the larger terms in these expansions are

$$K(z)|_{z\to 1} \approx -\frac{1}{2}\ln(1-z)+\ln 4 \tag{4.8}$$

$$E(z)|_{z\to 1} \approx 1 \tag{4.9}$$

Which we introduce into equation (4.5)

$$A_\varphi \approx \left(\frac{\mu_0}{4\pi}\right)2I\left(\frac{1}{2}\ln\frac{16}{(1-k)}-2\right) \tag{4.10}$$

where we have substituted r ≈ R in the loop. We know proceed to evaluate 1-k on the inside of the wire. We allow r= R+ ρ where ρ< a (the radius of the loop). Here we find the Taylor series expansion of k is

$$k \approx 1-\frac{\rho^2}{4R^2}+\frac{\rho^3}{4R^3}+\ldots \tag{4.11}$$

Substituting in equation (4.10) and taking only the term $1-k\approx(\rho/2R)^2$

$$A_\phi \approx \left(\frac{\mu_0 I}{2\pi}\right)\left(\ln\frac{8R}{\rho}-2\right) \tag{4.12}$$

Integrating first only on the area of cross section

$$\begin{aligned}\iint A_\phi J_\phi \rho' d\phi' d\rho' &= J_\phi \iint A_\phi \rho' d\phi' d\rho' \\ &= \left(\frac{\mu_0 I}{2\pi}\right)\left(\frac{I}{\pi a^2}\right)\iint \left(\ln\frac{8R}{\rho'} - 2\right)\rho' d\phi' d\rho' \\ &= \left(\frac{\mu_0 I}{2\pi}\right)\left(\frac{I}{\pi a^2}\right)(2\pi)\int \left(\ln\frac{8R}{\rho'} - 2\right)\rho' d\rho'\end{aligned}$$

Since $$\int [x\ln(8R/x) - 2x]dx = \frac{x^2\ln(8R/x)}{2} - \frac{3x^2}{4}$$

therefore
$$\begin{aligned}\frac{1}{2}\iint A_\phi J_\phi \rho' d\phi' d\rho' &= \left(\frac{\mu_0 I}{4\pi}\right)\frac{I}{\pi a^2}(2\pi)\frac{a^2}{2}\left[\ln(8R/a) - \frac{3}{2}\right] \\ &= \left(\frac{\mu_0 I^2}{4\pi}\right)\left[\ln(8R/a) - \frac{3}{2}\right]\end{aligned} \tag{4.13}$$

Integrating along the wire

$$\begin{aligned}W_m &= 2\pi R \times \left(\frac{\mu_0 I^2}{4\pi}\right)\left[\ln(8R/a) - \frac{3}{2}\right] \\ &= \left(\frac{\mu_0 I^2}{2}\right)R\left[\ln(8R/a) - \frac{3}{2}\right] \\ &= L\frac{I^2}{2}\end{aligned} \tag{4.14}$$

which gives the inductance of a single turn to be

$$L = \mu_0 R\left[\ln(8R/a) - \frac{3}{2}\right] \tag{4.15}$$

Chapter 5

Analysis of Inductor Geometries and Results

The purpose of this work is to examine inductor geometries which may be fabricated on-chip and find the best option based on calculations of mutual coupling with the external coil. However, in order that these coupling calculations may be considered reliable, we need to first validate the results obtained for simpler structures via measurements or known calculation methods. If the computational results are in good agreement with the measurement results, the validity of the computational method will be established and it may be used to confidently predict the inductance values of various structures with reasonable accuracy and speed.

Test Structures and Results

1) Circular Spiral Inductor(Circular Cross Section)

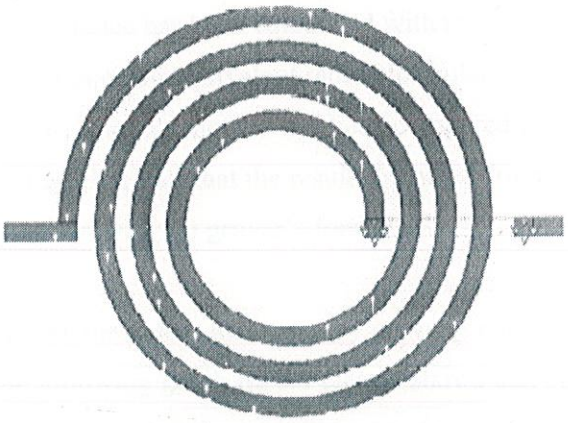

Figure 5.1
Circular Spiral Inductor

To test the validity of our assumption for the dimensions of on-chip inductors, we perform the calculations for the approximate range of values for the various on-chip dimensional parameters – line width W, metallization thickness T, distance of separation D and length of segments L.
In the above approximation, we consider the worst case scenario for estimating the value of D. Since smaller values of D will lead to larger error, we take the smallest value of D expected, which is the track separation between on-chip inductor segments. The track separation is assumed to be equal to the line width, which is generally the case. The specific case we shall consider for our calculations is that of two circular segments as shown in Figure 5.1 and compare the values of mutual inductance obtained to research paper.

For the on-chip inductors, the values of the dimensional parameters are approximated to be in the following range:

D ≈ 25μm; W ≈ 25μm; T ≈ 0.3μm; L ≈ 1.25mm → 5mm

In the table 5.1 the mutual inductance has been calculated with respect to variation in length of the inductor from 1.25mm to 5mm using equivalent radius formulation. In the following graph the result obtained from equivalent radius method has been compared to estimated value of grover's formula. The graph fig 5.1 shows that the results obtained from equivalent radius method are in close approximation with the grover's formula.

In the table 5.2 the error between the values estimated by grover's equation and equivalent radius method has been shown. The following graph fig 5.1 clearly shows that equivalent radius method provides result in close approximation but the error increases for the higher radius.

	Length(metres)	l1 and l2(H)	mutual inductace(H)
R1	0.00125	6.63524E-10	7.1948E-10
R2	0.001407	7.80156E-10	
R1	0.0015	8.50925E-10	9.09907E-10
R2	0.001657	9.72977E-10	
R1	0.002	1.24964E-09	1.31336E-09
R2	0.002157	1.38034E-09	
R1	0.003	2.11774E-09	2.18809E-09
R2	0.003157	2.26077E-09	
R1	0.0035	2.5786E-09	2.65145E-09
R2	0.003657	2.72636E-09	
R1	0.004	3.0538E-09	3.12881E-09
R2	0.004157	3.20567E-09	
R1	0.005	4.04039E-09	4.119E-09
R2	0.005157	4.19914E-09	

Table 5.1

Table showing Mutual Inductance

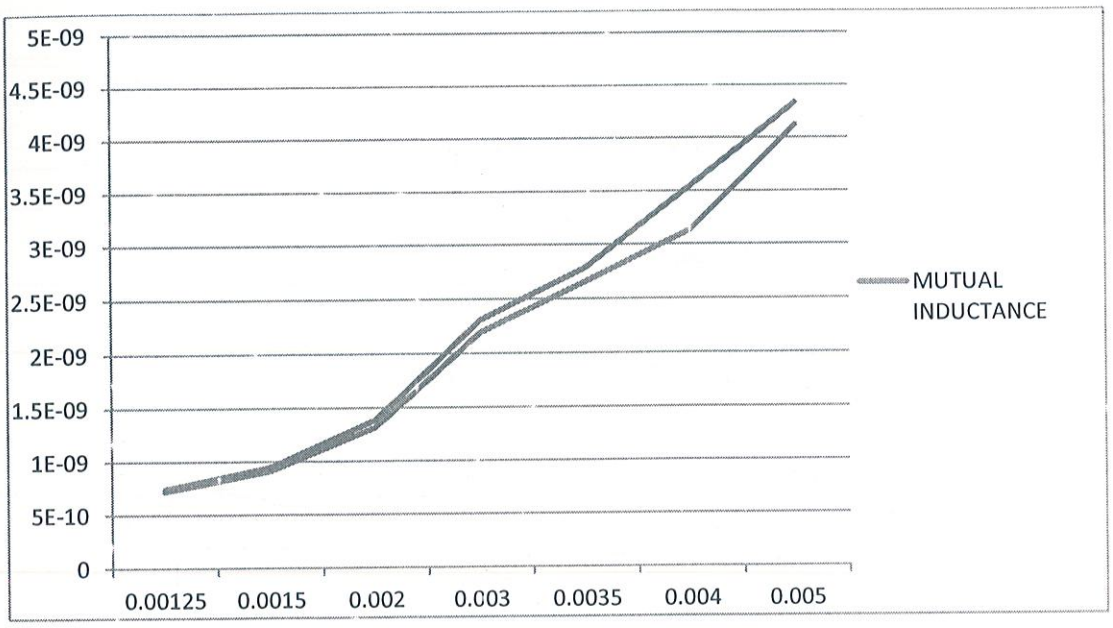

Figure 5.2

Figure showing the comparison between calculated value and Etd values

Radius	mutual inductance(H)	ETD VALUES(H)	ERROR %
R1	7.1948E-10	7.40E-10	2.77291302
R2			
R1	9.09907E-10	9.44E-10	3.611579104
R2			
R1	1.31336E-09	1.38E-09	4.82873702
R2			
R1	2.18809E-09	2.30E-09	4.865769
R2			
R1	2.65145E-09	2.78E-09	4.62403783
R2			
R1	3.12881E-09	3.54E-09	11.7263951
R2			
R1	4.119E-09	4.33E-09	4.872934854
R2			

Table 5.2

Table shows the percentage error of mutual inductance

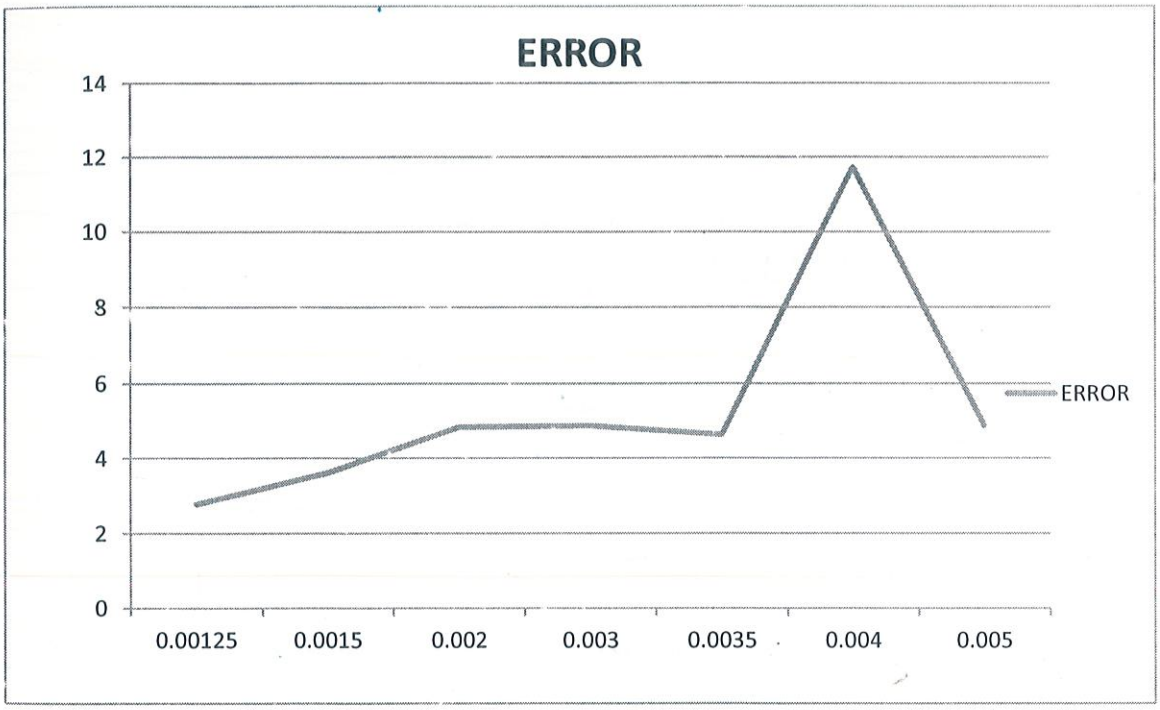

Figure 5.3

Figure shows the error percentage graph

No. of loops	Total Self Inductance
5	1.13E-08
6	1.48E-08
7	1.78E-08
8	1.88E-08

Table 5.3

Above table shows the total self Inductance of Circular Spiral Inductor

No. of loops	Inductance (Calculated) (H)	Inductance (Empirical)(H)	Error(%)
5	1.13E-08	1.05E-08	-6.94E+00
6	1.38E-08	1.33E-08	-3.77E+00
7	1.67E-08	1.64E-08	-1.66E+00
8	1.88E-08	1.85E-08	-1.55E+00

Table 5.4

Table Shows the comparison between the calculated and empirical values and percentage error

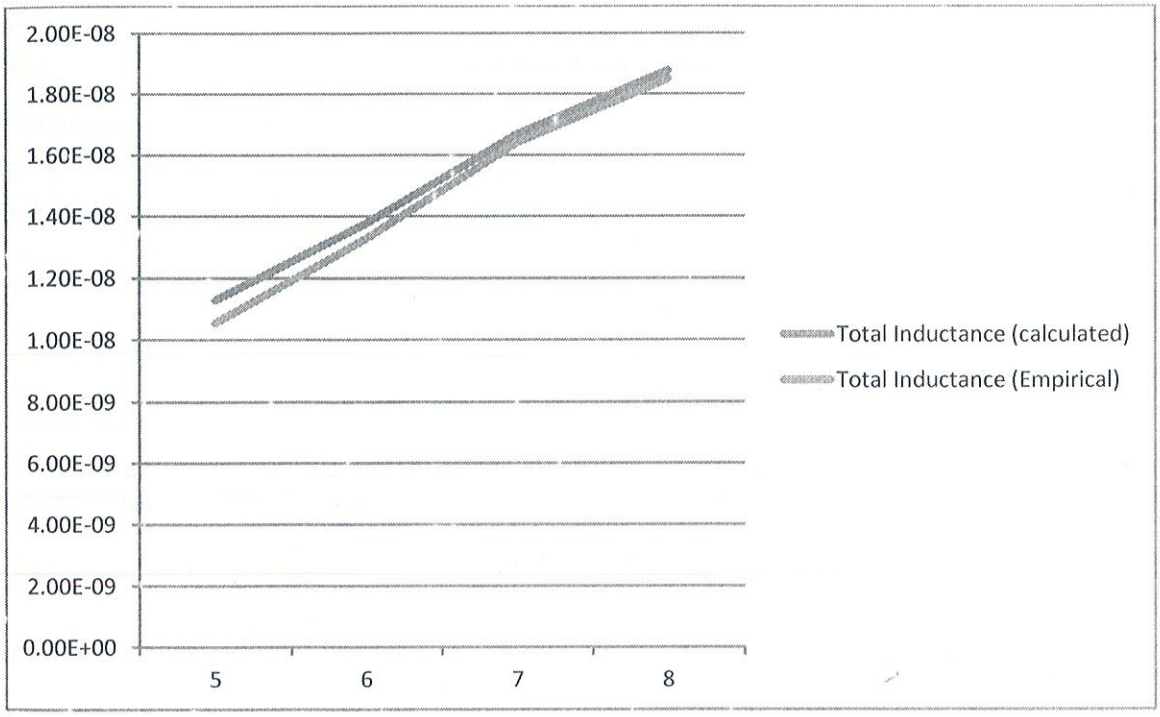

Figure 5.4

Comparision between total inductance (calculated) and (empirical)

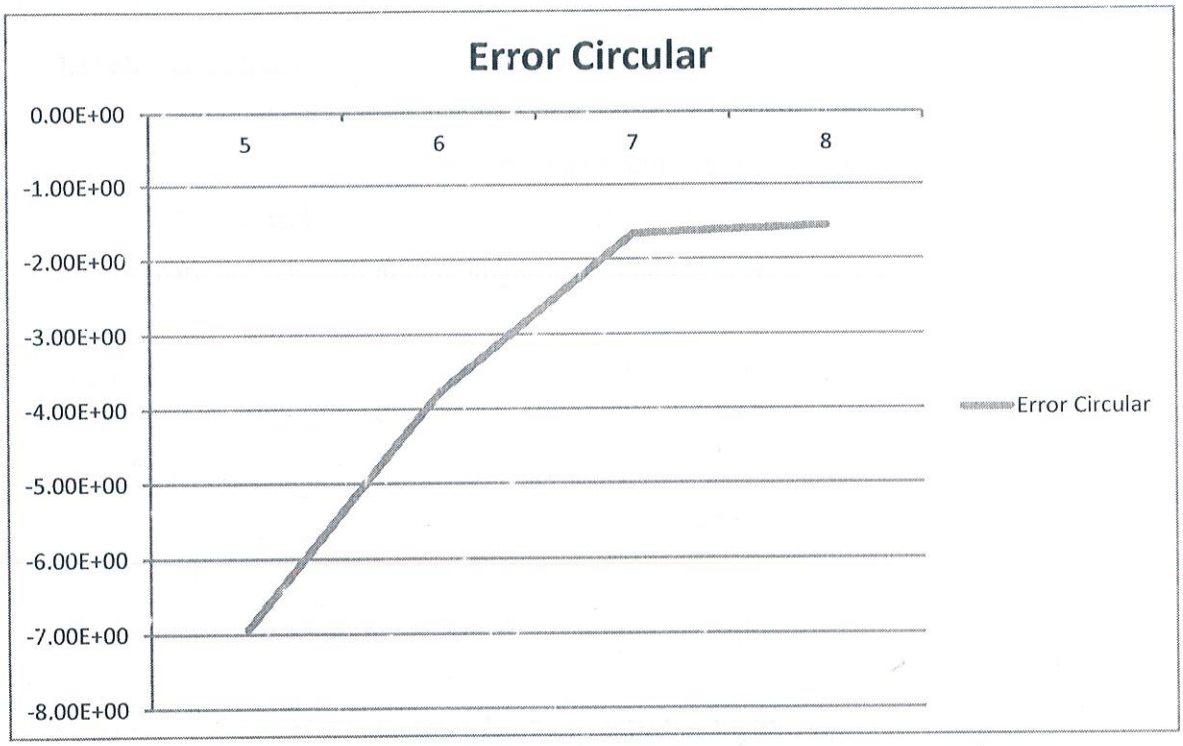

Figure 5.5

Error between empirical and calculated total inductance

2) Circular Spiral Inductor (Square Cross Section)

To test the validity of our assumption for the dimensions of on-chip inductors, we perform the calculations for the approximate range of values for the various on-chip dimensional parameters – line width W, metallization thickness T, distance of separation D and length of segments L. In the above approximation, we consider the worst case scenario for estimating the value of D. Since smaller values of D will lead to larger error, we take the smallest value of D expected, which is the track separation between on-chip inductor segments. The track separation is assumed to be equal to the line width, which is generally the case. The specific cases we shall consider for our calculations is that of two circular segments as shown in Fig. and compare the values of mutual inductance obtained to research paper.

For the on-chip inductors, the values of the dimensional parameters are approximated to be in the following range:

$D \approx 25\ \mu m$; $W \approx 25\ \mu m$; $T \approx 0.3\mu m$; $L \approx 1.25mm \rightarrow 5mm$

In the table 5.3 the mutual inductance has been calculated with respect to variation in length of the inductor from 1.25mm to 5mm using equivalent radius formulation. In the following graph the result obtained from equivalent radius method has been compared to estimated value of grover's formula. The graph fig 5.4 shows that the results obtained from equivalent radius method is in close approximation with the grover's formula .

In the table 5.4 the error between the values estimated by grover's equation and equivalent radius method has been shown. The following graph fig 5.5 clearly shows that equivalent radius method provides result in close approximation but the error increases for the higher radius.

Radius	Length(m)	CIRCULAR INDUCTANCE(H)	MUTUAL INDUCTANCE(H)
R1	0.00125	7.36727E-10	7.99E-10
R2	0.001407	8.66227E-10	
R1	0.0015	9.44803E-10	1.01E-09
R2	0.001657	1.08032E-09	
R1	0.002	1.38751E-09	1.46E-09
R2	0.002157	1.53262E-09	
R1	0.003	2.35138E-09	2.43E-09
R2	0.003157	2.51019E-09	
R1	0.0035	2.86308E-09	2.94E-09
R2	0.003657	3.02715E-09	
R1	0.004	3.39071E-09	3.47E-09
R2	0.004157	3.55933E-09	
R1	0.005	4.48615E-09	4.57E-09
R2	0.005157	4.66242E-09	

Table 5.5

Calculated Self inductance and Mutual inductance

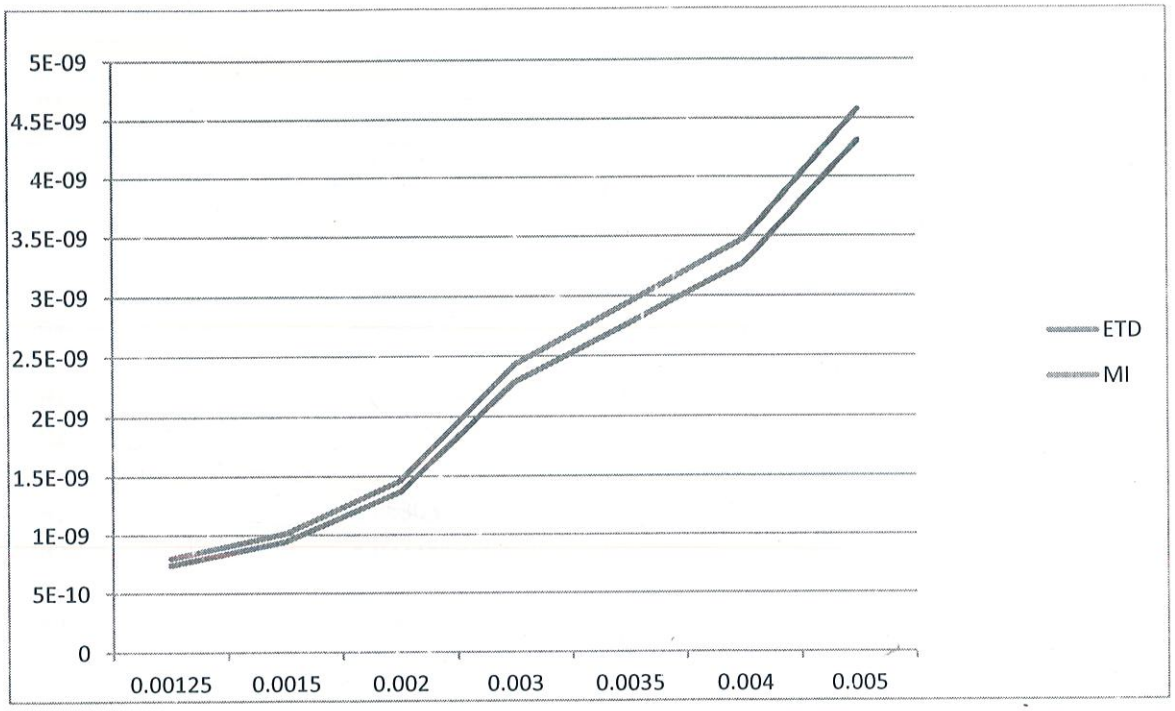

Figure 5.6

Comparision between calculated values and etd values

Radius	CIRCULAR INDUCTANCE(H)	MUTUAL INDUCTANCE (H)	ERROR %
R1	7.36727E-10	7.99E-10	-8.260076509
R2	8.66227E-10		
R1	9.44803E-10	1.01E-09	-7.681821775
R2	1.08032E-09		
R1	1.38751E-09	1.46E-09	-7.00881581
R2	1.53262E-09		
R1	2.35138E-09	2.43E-09	-6.441987532
R2	2.51019E-09		
R1	2.86308E-09	2.94E-09	-6.314656074
R2	3.02715E-09		
R1	3.39071E-09	3.47E-09	-6.234925606
R2	3.55933E-09		
R1	4.48615E-09	4.57E-09	-6.154172675
R2	4.66242E-09		

Table 5.6

Error percentage

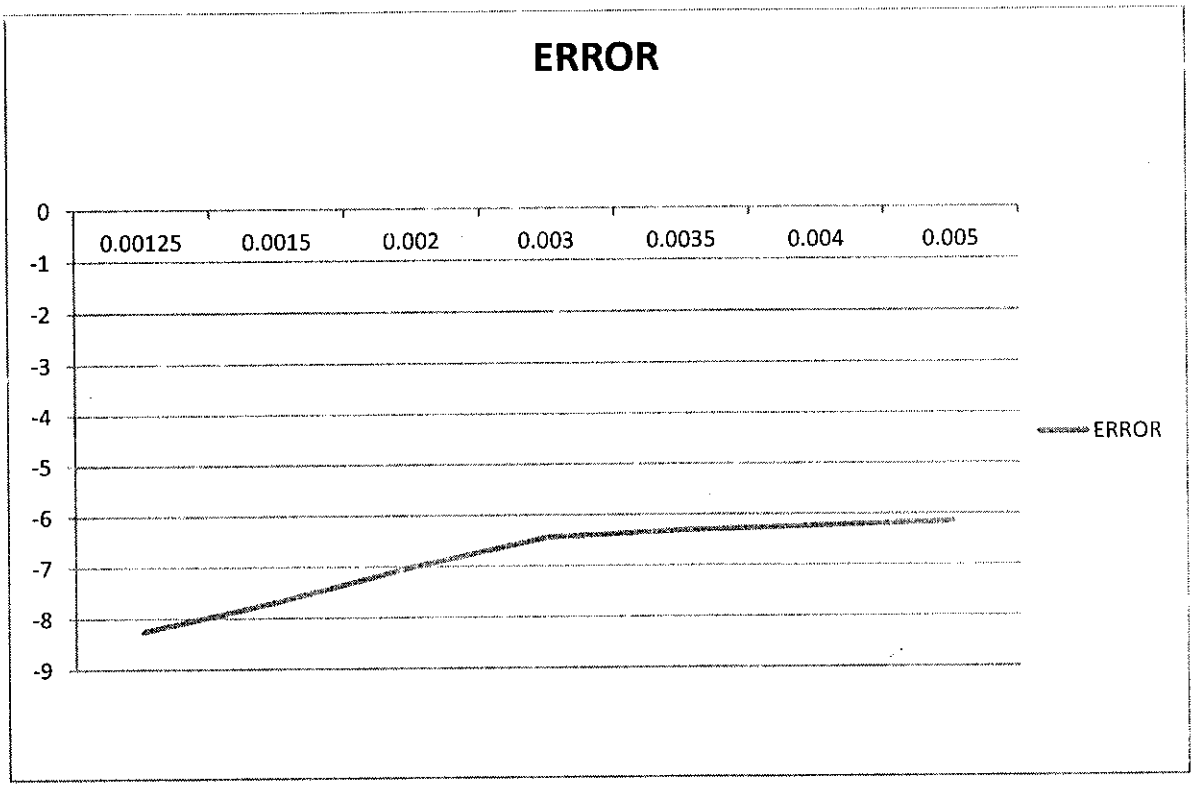

Figure 5.7

Graph of percentage error

3) Square Spiral Inductor (Circular Cross Section)

To test the validity of our assumption for the dimensions of on-chip inductors, we perform the calculations for the approximate range of values for the various on-chip dimensional parameters – line width W, metallization thickness T, distance of separation D and length of segments L. In the above approximation, we consider the worst-case scenario for estimating the value of D. Since smaller values of D will lead to larger error, we take the smallest value of D expected, which is the track separation between on-chip inductor segments. The track separation is assumed to be equal to the line width, which is generally the case. The specific case we shall consider for our calculations is that of two circular segments as shown in Fig. and compare the values of mutual inductance obtained to research paper.

For the on-chip inductors, the values of the dimensional parameters are approximated to be in the following range:

$D \approx 25\ \mu m$; $W \approx 25\ \mu m$; $T \approx 0.3\mu m$; $L \approx 1.25mm \rightarrow 5mm$

In the table 5.3 the mutual inductance has been calculated with respect to variation in length of the inductor from 1.25mm to 5mm using equivalent radius formulation. In the following graph the result obtained from equivalent radius method has been compared to estimated value of grover's formula. The graph fig 5.4 shows that the results obtained from equivalent radius method are in close approximation with the grover's formula.

In the table 5.4 the error between the values estimated by grover's equation and equivalent radius method has been shown. The following graph fig 5.5 clearly shows that equivalent radius method provides result in close approximation but the error increases for the higher radius.

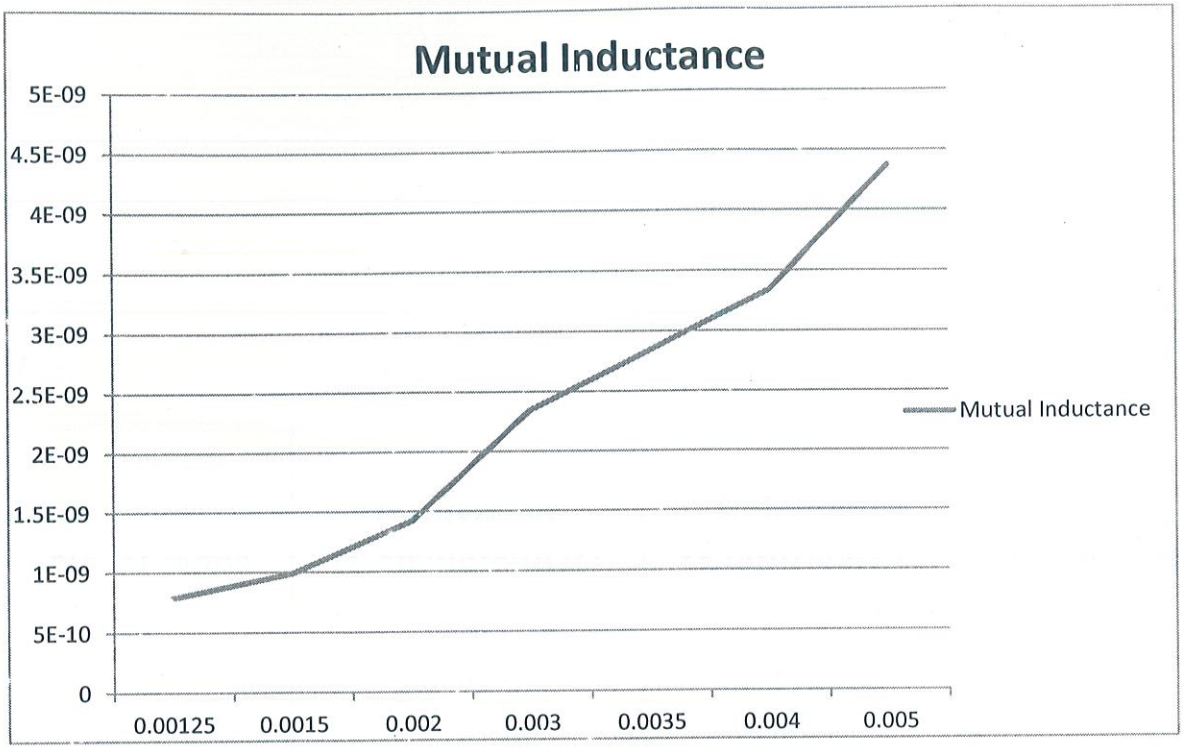

Figure 5.8

Mutual inductance of square spiral inductor

Total Self Inductance for Square Spiral

No. of loops	Total Self Inductance (H)
5	1.25E-08
6	1.76E-08
7	1.85E-08
8	2.35E-08

Table 5.7

No. of loops	Inductance (Calculated)(H)	Inductance (Empirical)(H)	Error (%)
5	1.25E-08	1.27E-08	1.24E+00
6	1.66E-08	1.62E-08	-2.32E+00
7	1.85E-08	1.94E-08	4.47E+00
8	2.35E-08	2.33E-08	-8.62E-01

Table 5.8

Comparision between calculated and empirical inductance and its error

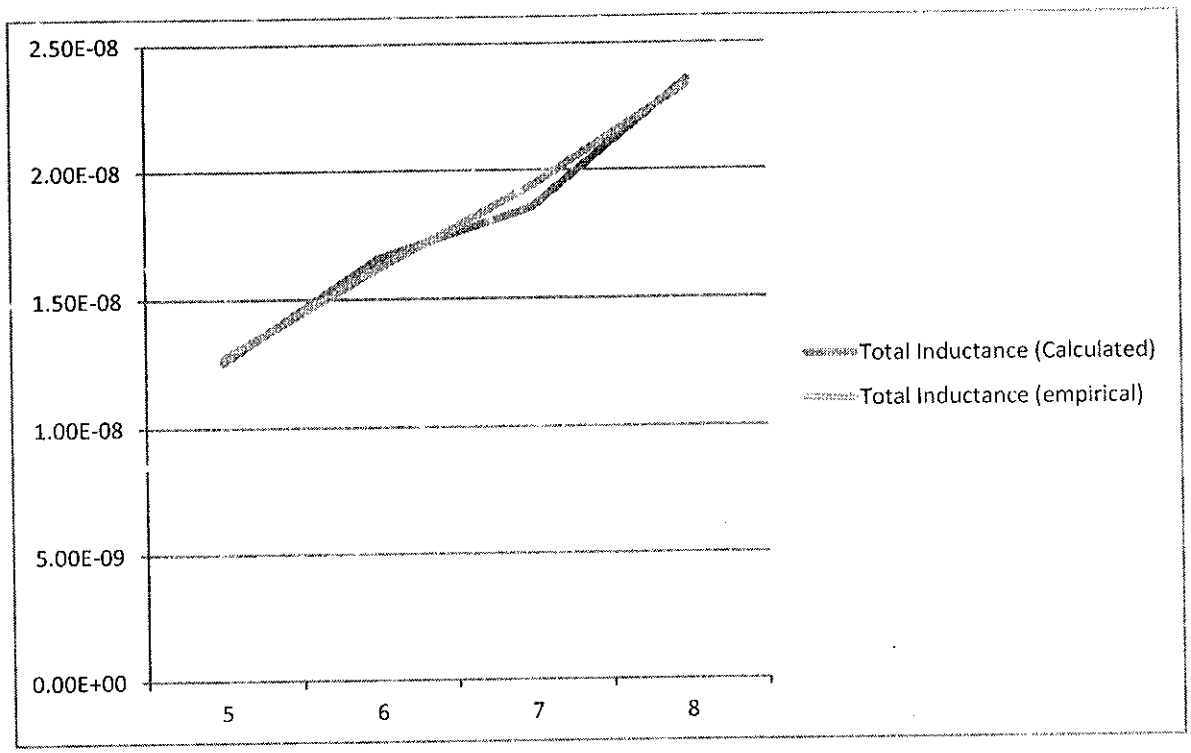

Figure 5.9

Comparision between calculated and empirical total inductance

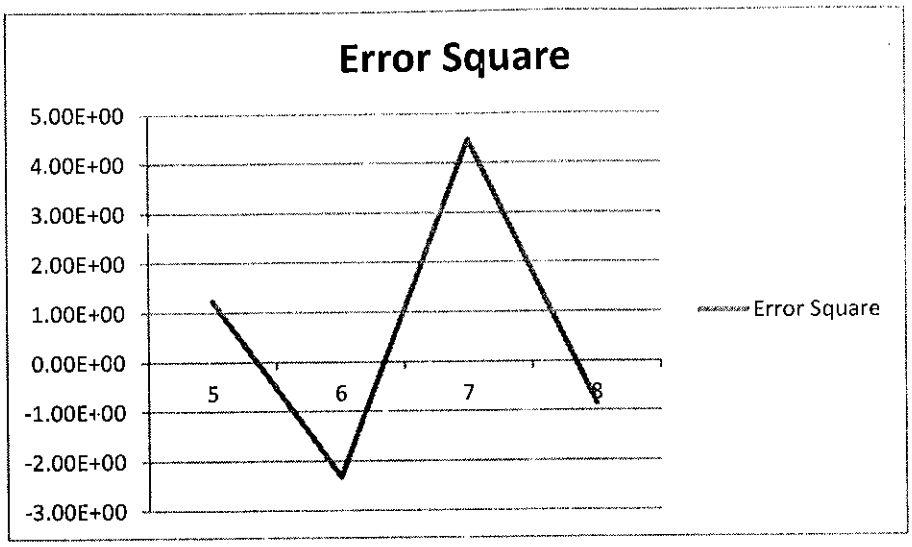

Figure 5.10

Percentage error in square spiral inductor

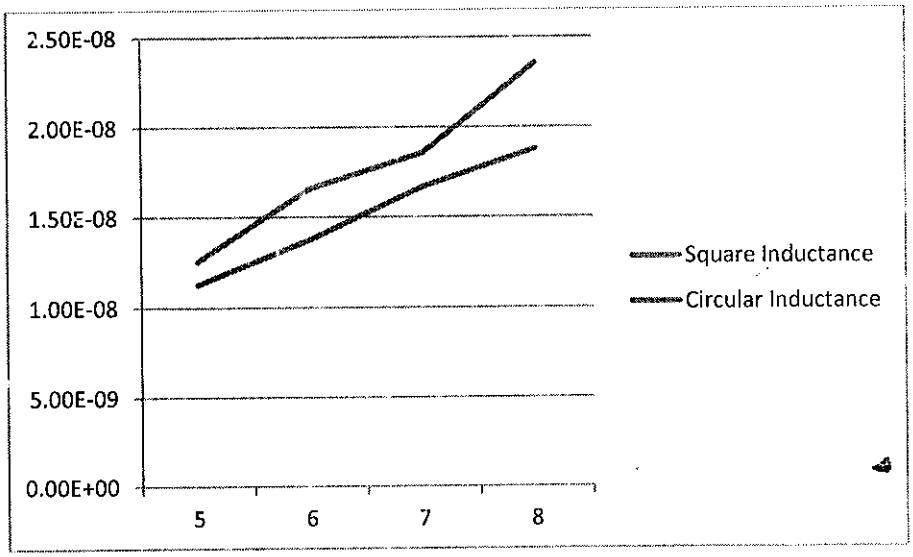

Figure 5.11

Graphical comparision of total inductance

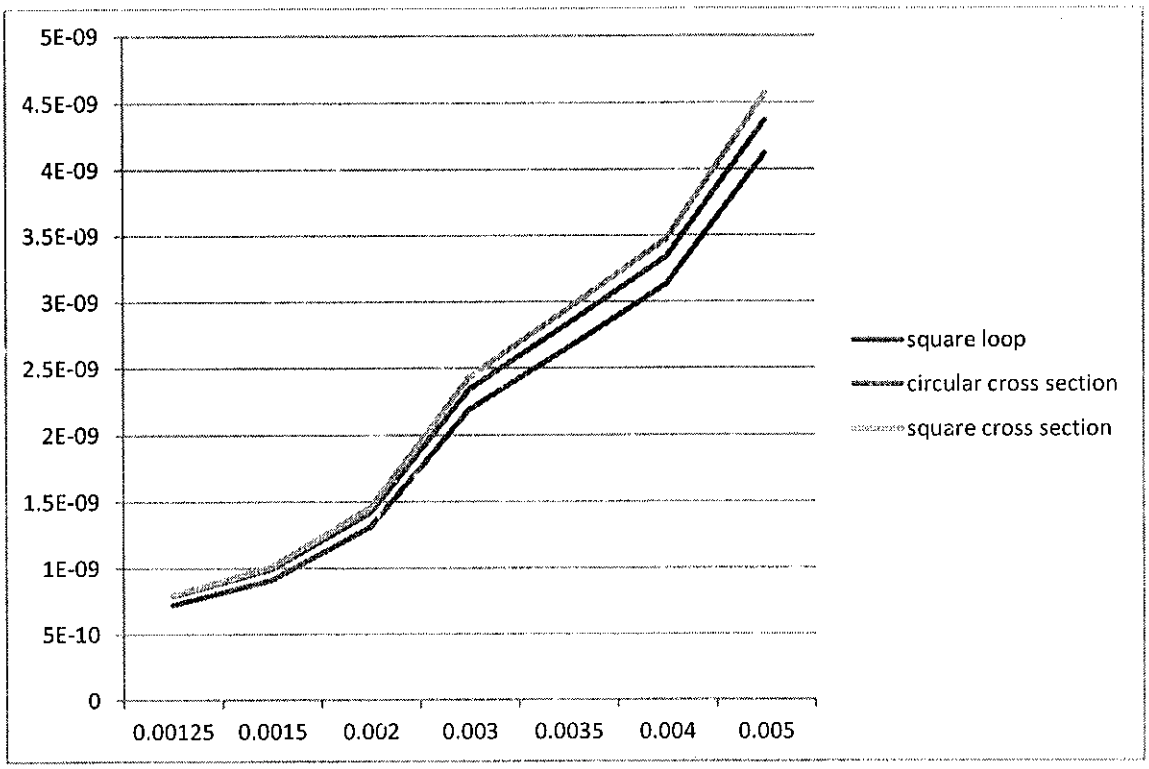

Figure 5.12

Graphical comparision of mutual inductance

CHAPTER 6
CONCLUSION

This thesis has developed a computational method for inductance predictions of inductors and investigated novel geometries for spiral inductor. This chapter summarizes the major contributions of this work and identifies areas that merit future study.

Present work provides detail information on integrated inductors. Construction and modeling of an IC inductor has been discussed briefly. The equations that are used for inductor calculations are analyzed. Inductor behavior with respect to its internal dimensions such as d, w, t, and l is calculated using equivalent radius method.

Specific conclusions have been drawn from the plots after careful observations. While working on the design procedure, it was observed that some of the equations believed to be accurate are conducive for design. This can be explained by comparing results with Grover's equation.

The graphs clearly show that the results are in good approximation to the Grover's equation, although the error increase as the net radius of spiral inductor increases. But in case spiral inductor with square cross area the results are in better approximation with results.

REFERENCES

[1] A.A. Abidi, "RF CMOS comes of age," *IEEE J. Solid-State Circuits*, vol. 39, no. 4, pp. 549-561, Apr. 2004.

[2] J.Y.-C. Chang, A.A. Abidi and M. Gaitan, "Large suspended inductors on silicon and their use in a 2-μm CMOS RF amplifier," *IEEE Electron Device Lett.*, vol. 14, no. 5, pp. 246-248, May 1993.

[3] J.N. Burghartz, D.C. Edelstein, M. Soyuer, H.A. Ainspan and K.A. Jenkins, "RF circuit design aspects of spiral inductors on silicon," *IEEE J. Solid-State Circuits*, vol. 33, no. 12, pp. 2028-2034, Dec. 1998.

[4] N.M. Nguyen and R.G. Meyer, "Si IC-compatible inductors and LC passive filters," *IEEE J. Solid-State Circuits*, vol. 25, no. 4, pp. 1028- 1031, Aug. 1990.

[5] R.B. Merrill, T.W. Lee, H. You, R. Rasmussen and L.A. Moberly, "Optimization of high Q integrated inductors for multi-level metal CMOS," *IEDM 1995*, pp. 38.7.1-38.7.3.

[6] J.N. Burghartz, M. Soyuer and K. Jenkins, "Microwave inductors and capacitors in standard multilevel interconnect silicon technology," *IEEE Trans. Microwave Theory Tech*, vol. 44, no. 1, pp. 100-103, Jan. 1996.

[7] K.B. Ashby, I.A. Koullias, W.C. Finley, J.J. Bastek and S. Moinian, "High Q inductors for wireless applications in a complementary silicon bipolar process," *IEEE J. Solid-State Circuits*, vol. 31, no. 1, pp. 4-9, Jan. 1996.

[8] C. Yue and S. Wong, "On-chip spiral inductors with patterned ground shields for Si-based RF IC's," *IEEE J. Solid State Circuits*, vol. 33, no. 5,pp. 743-752, May 1998.

[9] J.Y. Park and M.G. Allen, "High Q spiral-type microinductors on silicon substrates," *IEEE Trans. Magn.*, vol. 35, no. 5, pp. 3544-3546, Sep. 1999.

[10] H. Jiang, Y. Wang, J.L. Andrew and N.C. Tien, "On-chip spiral inductors suspended over deep copper-lined cavities," *IEEE Trans. Microwave Theory Tech.*, vol. 48, no. 12, pp. 2415-2423, Dec. 2000.

[11] J.B. Yoon, Y.S. Choi, B.I. Kim, Y. Eo and E. Yoon, "CMOS-compatible surface-micro machined suspended-spiral inductors for multi-GHz silicon RF ICs," *IEEE Electron Device Lett.*, vol. 23, no. 10, pp. 591-593, Oct.2002.

[12] G.M. Rebeiz, *RF MEMS: Theory, Design and Technology*, New York: Wiley, 2003.

[13] C.P. Yue, C. Ryu, J. Lau, T.H. Lee and S.S. Wong, "A physical model for planar spiral inductors on silicon," *Techn. Dig. IEDM*, pp. 155-158, 1996.

[14] C.P. Yue and S.S. Wong, "Physical modeling of spiral inductors on silicon," *IEEE Trans. on Electron Devices*, vol. 47, no. 3, pp. 560-568, Mar. 2000.

[15] K.B. Ashby, I.A. Koullias, W.C. Finley, J.J. Bastek and S. Moinian, "High Q inductors for wireless applications in a complementary silicon bipolar process," *IEEE J. Solid-State Circuits*, vol. 31, no. 1, pp. 4-9, Jan. 1996.

[16] S.S. Mohan, M. Hershenson, S.P. Boyd and T.H. Lee, "Simple accurate expressions for planar spiral inductances," *IEEE J. Solid-State Circuits*, vol. 34, no. 10, pp. 1419-1424, Oct. 1999.

[17] J.R. Long and M.A. Copeland, "The modeling, characterization, and design of monolithic inductors for silicon RF IC's," *IEEE J. Solid-State Circuits*, vol. 32, no. 3, pp. 357-369, Mar. 1997.

[18] A. Niknejad, ASITIC: Analysis and Simulation of Spiral Inductors and Transformers for ICs, Univ. California, Berkeley, [Online]. Available: http://rfic.eecs.berkeley.edu/~niknejad/asitic.html.

[19]*em*, Sonnet Software, Inc. 100 Elwood Davis Road, North Syracuse, NY 13212, USA.

[20] Agilent Momentum, Agilent Technologies, 1400 Fountaingrove Parkway, Santa Rosa, CA 95403-1799, USA.

[21] C.-Y. Lee, T.-S.Chen, J.D.-S.Deng and C.-H. Kao, "A simple systematic spiral inductor design with perfected Q improvement for CMOS RFIC application," *IEEE Trans. Microwave Theory Tech.*, vol. 53, no. 2, pp. 523-528, Feb. 2005.

[22] M. Hershenson, S.S. Mohan, S.P. Boyd and T.H. Lee, "Optimization of inductor circuits via geometric programming," *Proc. 36th Design Automation Conf.*, pp. 994-998, Jun. 1999.

[23] G. Stojanovic and L. Zivanov, "Comparison of optimal design of different spiral inductors," *24th Int. Conf. Microelectronics*, vol. 2, pp. 613-616, May 2004.

[24] Y. Zhan and S.S. Sapatnekar, "Optimization of integrated spiral inductors using sequential quadratic programming," *2004 Design, Automation and Test in Europe Conf. Exhibition*, vol. 1, pp. 622-627, Feb. 2004.

[25] A. Nieuwoudt and Y. Massoud, "Multi-level approach for integrated spiral inductor optimization," *Proc. 42nd Design Automation Conf.*, pp. 648-651, Jun. 2005.